OPEN ACCESS
IOP Publishing

Letters
Journal of Physics D: Applied Physics

J. Phys. D: Appl. Phys. **55** (2022) 35LT01 (7pp)
https://doi.org/10.1088/1361-6463/ac782f

Letter

A thermophone-based bridge circuit for the measurement of electrical and thermal properties of thin films

D M Tatnell, M S Heath, A P Hibbins and D W Horsell*

Department of Physics and Astronomy, University of Exeter, Stocker Road, Exeter EX4 4QL, United Kingdom

E-mail: D.W.Horsell@exeter.ac.uk

Received 28 January 2022, revised 5 June 2022
Accepted for publication 13 June 2022
Published 22 June 2022

Abstract

Sound can be generated via modulated Joule heating of thin conductive films. Its amplitude and phase are sensitive to the electrical and thermal properties of the film. Here we show how such sound can be used to measure and quantify these properties. In particular, we experimentally determine the relative conductances of electrical paths in a multi-branched thin film, which can then be used to find the temperature dependence of the film conductance. This is achieved by nullifying the sound at a given point in the sound field using simple voltage control. This method, essentially an acoustic analogue of an electrical bridge circuit, is advantageous since it allows for electrical and thermal properties to be measured simultaneously. These attributes benefit the characterisation of complex circuit architectures, as well as thermal sensing.

Supplementary material for this article is available online

Keywords: thermoacoustics, thermophone, acoustics, bridge

(Some figures may appear in colour only in the online journal)

1. Introduction

A thermophone is a device that generates sound due to an oscillating heat source within it [1]. The heat transferred to the surrounding medium results in a pressure change that propagates away from the device as sound. Thermophones are simple devices, typically consisting of a single electrically conductive element that dissipates Joule heat from an alternating current source. They are non-resonant, broadband, and can be easily fabricated using standard lithographic techniques. The Joule power, P, is related to the driving voltage, V, and element conductance, G, through $P = GV^2$. For a linear conductor, this square dependence on the voltage causes sound to be generated at the second harmonic of a sinusoidal source frequency, f. Any electrical nonlinearity in the conductor can be quantified through any additional frequency components generated by the thermophone [2].

To date, the majority of thermophone research has focused on addressing the relatively poor conversion efficiency of source power into sound [3–5]. However, for many potential applications this efficiency is irrelevant: the distinctive

* Author to whom any correspondence should be addressed.

mechanism of sound production has been shown to already have use in non-destructive evaluation [6], active noise cancellation [7], signal heterodyning [2], and ultrasonic phased arrays [8].

In this work, we demonstrate that the sound generated by a thermophone consisting of multiple conductive thin film branches can be used to determine its electrical and thermal properties. We begin with a general case of a device consisting of three branches, each producing sound, figure 1(a). The sound is used to measure the relative electrical conductance of each of the branches. Then, to allow for the absolute value of this conductance to be determined, we consider the case where only two of these branches produce sound and the third is an arbitrary load of unknown conductance. Finally, we demonstrate how multi-branch measurements can be extended to include thermal effects such as the temperature dependence of the electrical conductance. The properties of the film are found through balancing the sound output from the different branches of the device. In this sense, our device functions in a similar way to an electrical bridge circuit. Bridge circuits have myriad applications in areas such as sensor design [9–11]. Here we show that this 'thermophonic bridge' has several distinct advantages over its traditional electrical counterparts. The lack of internal electrical connections is useful in situations where individual electrical contact with conducting branches may not be feasible. The frequency dependence of the spatial response of the sound also offers opportunities to enhance precision via beam shaping [8].

2. Thermophonic bridge theory

In a simple thermodynamic model, the acoustic pressure in air generated by a point-like thermophone is given by [12]

$$p \propto \frac{Pf_2}{r}, \tag{1}$$

where P is the (complex) Joule power, $f_2 = 2f$ is the second harmonic of the driving voltage of frequency f, and r is the radial distance from the thermophone. (The proportionality constant depends on the thermal conductivity and heat capacity of the system and is not important for the current work; supplementary S1 for derivation.) For devices consisting of multiple millimetre-scale thermophonic elements, thermal coupling between elements at acoustic frequencies is negligible because the decay length of thermal waves ($\sqrt{\alpha/\pi f_2}$, where α is the thermal diffusivity) is several orders of magnitude shorter than the device dimensions. As such, the elements can be treated as independent acoustic sources. There is, however, electrical coupling, depending on the circuit configuration [8]. The operation of the thermophonic bridge is based upon this coupling. A useful quantity is the total far-field acoustic pressure,

$$p_{\text{total}} = \oint_S p \, \mathrm{d}S, \tag{2}$$

where S is a surface enclosing the device. Modelling a device as a collection of planar acoustic sources with finite dimensions, the above integral becomes difficult and often has no closed-form solution. Instead, if the device dimensions are sufficiently small relative to the acoustic wavelength then it can be assumed to behave as a point-like source, for which p has no angular dependence. In this case, equation (1) suggests that $p_{\text{total}} \propto P_{\text{total}}$, the sum of the Joule power from all thermophone sources. Therefore, the total sound pressure can be used as a measure of the total Joule power in the system. It is this measurement of the total Joule power that allows for the electrical properties of the device to be determined. Decreasing the wavelength, such that it is comparable to the device dimensions, introduces error into this result due to diffractive effects.

Consider the device shown in figure 1(a). Two different ac voltages, V_1 and V_2, are applied to branches 1 and 2, respectively. The third branch is held at 0 V. This can be modelled as a simple circuit, figure 1(b), with each branch represented by a conductive element, $G_{1,2,3}$. If V_1 and V_2 are both sinusoidal with frequency f and phase difference φ, the total Joule power $(P_1 + P_2 + P_3)$ dissipated by the device is

$$P_{\text{total}} = \left(1 - \frac{G_1}{\Sigma}\right) G_1 |V_1|^2 + \left(1 - \frac{G_2}{\Sigma}\right) G_2 |V_2|^2 \mathrm{e}^{2\mathrm{i}\varphi} - 2\frac{G_1 G_2}{\Sigma} |V_1||V_2| \mathrm{e}^{\mathrm{i}\varphi}, \tag{3}$$

where $\Sigma \equiv G_1 + G_2 + G_3$ (supplementary S2). Here V_1, V_2 and P_{total} are rms quantities, since these are what are measured experimentally. The thermophone sources in this case are electrically coupled, since the Joule power dissipated in each branch is dependent on the conductance of all other branches. Due to the proportionality between the total Joule power and total sound pressure, the total Joule power can be measured up to some constant by integrating the sound field generated by the device. Combining multiple measurements then allows for the constant of proportionality to be eliminated. Measurement of this quantity affords two bridging methods for determining the conductances of the branches.

The first, 'voltage-based' method involves changing the amplitudes of V_1 and V_2 with zero phase shift between them ($\varphi = 0$). From equation (3), it can be seen that the conductance ratios can be determined by measuring the total power when switching the two sources on or off (supplementary S3),

$$G_1 P_{\text{A}} = G_2 P_{\text{B}} = G_3 P_{\text{C}}, \tag{4}$$

where

$$\begin{aligned} P_{\text{A}} &\equiv -P_{1,0} + P_{0,1} + P_{1,1}, \\ P_{\text{B}} &\equiv P_{1,0} - P_{0,1} + P_{1,1}, \\ P_{\text{C}} &\equiv P_{1,0} + P_{0,1} - P_{1,1}. \end{aligned} \tag{5}$$

Here, $P_{x,y}$ is the total power (or total sound pressure) measured, where x and y define the on (1) or off (0) state of V_1 and V_2, respectively.

The second, 'phase-based' method involves changing both the amplitudes of V_1 and V_2, as well as their relative phase φ. In this case, it is possible to generate zero total power in

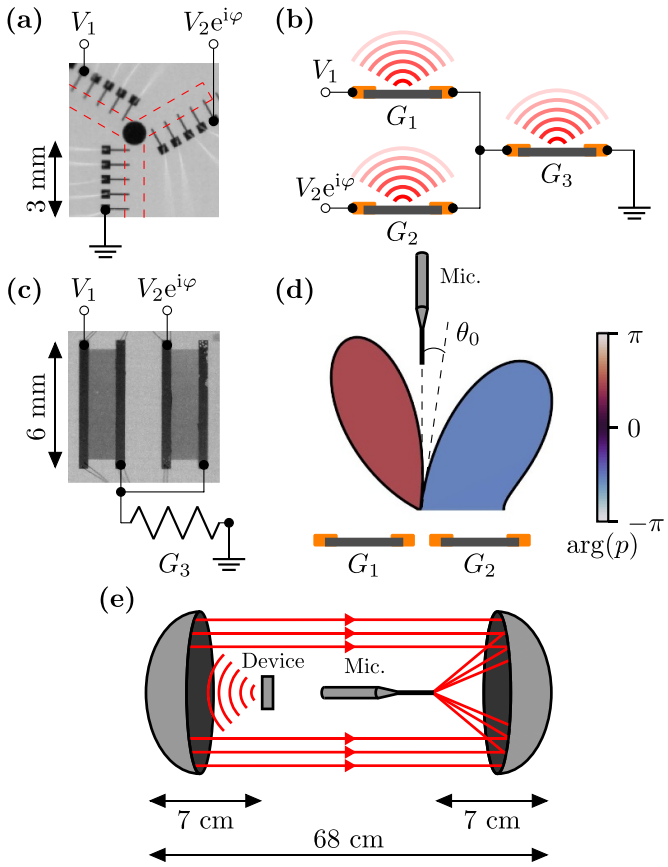

Figure 1. (a) Ambient thermal image of a three-branch ITO film (outlined with red dashed lines) with multiple gold contacts (solid black). The choice of contact along each branch allows its length (and, therefore, conductance) to be varied. (b) Thermophonic bridge circuit. Thin film branches of conductance $G_{1,2,3}$ produce sound via Joule heating due to two ac source voltages $V_{1,2}$. (c) Two-branch device consisting of ITO films of equal, known conductance. These are connected to ground via an external unknown conductance that does not produce sound. (d) Schematic of two-branch steering measurement, showing the directivity of the far-field sound produced by a two-branch bridge. The magnitude is indicated by the radial extent and the phase by the colour. When perfectly balanced, the directivity shows a null at $\theta_0 = 0$. This shifts as the bridge becomes unbalanced. The far-field directivity is measured by rotating the device relative to a microphone placed at a fixed distance. (e) Method for measuring the total sound. Two parabolic reflectors (radius 15 cm, depth 8 cm) collect the sound emitted from the device and focus it onto the microphone, allowing for the total sound produced to be determined with a single measurement.

equation (3) for finite voltage amplitudes. By substituting $x = \frac{|V_2|}{|V_1|}e^{i\varphi}$ and solving the resulting quadratic, this occurs when

$$\frac{|V_2|}{|V_1|}e^{i\varphi} = \frac{G_1 \pm G_1\sqrt{-G_3\Sigma/G_1G_2}}{G_1+G_3}, \tag{6}$$

(supplementary S4). At this point, there is finite power dissipation from each of the branches, but the total is zero due to phase cancellation. By measuring the values $(|V_2|/|V_1|)_0$ and φ_0 at this zero total power condition, the conductance ratios can be determined from equation (4), where instead

$$P_A \equiv \left(\frac{|V_1|}{|V_2|}\right)_0 - \cos\varphi_0\,,$$

$$P_B \equiv \left(\frac{|V_2|}{|V_1|}\right)_0 - \cos\varphi_0\,,$$

$$P_C \equiv \cos\varphi_0\,. \tag{7}$$

The sound field can also be used to measure the conductance of a branch that does not produce sound itself. Consider the same circuit as before, but now only branches 1 and 2 produce sound (figure 1(c)). For convenience, these are of equal conductance, G. Branch 3 is of unknown conductance, G_x, and does not produce sound. The total sound in this case is therefore proportional to the sum of the powers in branches 1 and 2. Again, the conductance ratios can be determined by tuning V_1, V_2 and φ such that $P_1 + P_2 = 0$ (supplementary S5), in which case

$$\frac{G_x}{G} = \frac{1+\sin\varphi_0}{\cos\varphi_0} - 1\,. \tag{8}$$

An alternative approach for the two-branch device is to consider the directionality of the far-field sound. When V_1, V_2 and φ are set to achieve zero total sound, the sound generated by the two acoustic branches must perfectly interfere, i.e. they have equal magnitude and opposite phase. Modelling the two branches as rectangular planar sources with separation d (supplementary S5) and width L, the far-field pressure magnitude is

$$|p| = \frac{2A}{r}\left|\mathrm{sinc}\left(\frac{kL}{2}\sin\theta\right)\cos\left(\frac{kd\sin\theta-\psi}{2}\right)\right|, \tag{9}$$

where k is the acoustic wavenumber, θ is the measurement angle from the axis normal to the device and ψ is the acoustic phase difference between the sources. For $P_1 + P_2 = 0$, $\psi = \pi$, resulting in a dipolar sound field (figure 1(d)). Changing the source parameters away from these values causes the field to become more monopolar. From equation (8), altering G_x causes a shift in the phase difference required for a dipole. In terms of the sound output from each branch, if φ is kept constant and G_x is increased then the phase difference between the two branches will change, while their magnitudes remain equal. This results in transition between dipolar and monopolar fields. Defining θ_0 as the angle at which there is a null in the sound field between the two major lobes of the dipole, it can be shown that

$$\theta_0 = \arcsin\left[\frac{\pi}{kd} + \frac{2}{kd}\arctan\left(-\frac{G_x(G_x+2G)}{2G(G_x+G)}\right)\right], \tag{10}$$

from which

$$\frac{G_x}{G} = \frac{1-\sin\left(\frac{kd\sin\theta_0-\pi}{2}\right)}{\cos\left(\frac{kd\sin\theta_0-\pi}{2}\right)} - 1\,, \tag{11}$$

where k is the acoustic wavenumber. Therefore, the conductance ratio can be determined directly by measuring the angle at which a null appears in the directivity of the far-field sound.

3. Measurements

Thermophones with three and two branches are shown in figures 1(a) and (c), respectively. (For details of fabrication, see supplementary S6.) The three-branch device consisted of a continuous indium tin oxide (ITO) thin film patterned into three, nominally identical radiating branches. Each branch had planar dimensions 3.0×0.5 mm with thickness 50 nm, and gold contacts were placed with pitch 0.5 mm along its length. By choosing which contact to connect to source and drain, the length of each branch was varied, thus changing its conductance. The additional contacts also allowed for differential voltage measurements to be performed on each branch, such that the Joule power could be measured electrically for direct comparison with the sound. The two-branch device consisted of two 7×2 mm rectangular films with separation 5 mm. These two branches were individually sourced, and connected to ground via a variable conductance.

Voltages V_1 and V_2 were sourced from individual phase-locked channels of a waveform generator (Rigol DG4102) and amplified (Rigol PA1011) to cause measurable Joule heating. Both electrical and acoustic measurements were taken using lock-in amplifiers, phase locked to the source (Signal Recovery 7124). Acoustic measurements were taken with a condenser microphone (Earthworks M50 with ZDT1022 preamp). The lock-in amplifier for the acoustic measurements was set to take measurements at the second harmonic of the source. Thermal measurements were taken with a thermal imaging camera (FLIR A655SC).

To quantify the electrical properties from the sound measurements, the proportionality between the total sound and total Joule power must be verified (equation (1)). This is frequency dependent due to diffractive effects caused by the finite size of the device. Experimentally, the challenge is to find a frequency that is low enough to minimise diffractive effects, whilst also providing a sufficiently high signal-to-noise ratio. The three-branch device was connected such that the lengths of the branches, hence their conductances, were equal. The phase was then swept across the range $-\pi \leqslant \varphi \leqslant \pi$, with $|V_1| = |V_2|$. A differential voltage measurement was taken along each of the branches, from which the total Joule power could be inferred. Integration measurements of the sound field were performed using a pair of parabolic reflectors to focus the sound to a single point, figure 1(e). The device was placed at the focal point of one of the reflectors and the microphone at the other. The reflectors were then placed opposite each other such that the sound emitted from the device was collected and focused onto the microphone. This is not a true measure of the total sound as the integration surface does not completely encompass the device; however, the proposed method is more time-efficient as it only involves a single measurement, rather than a full mapping of the far-field sound. This inevitably leads to some discrepancy between the measured and actual total sound, which can be minimised with suitable choice of frequency. Measurements were therefore performed to quantify the discrepancies between the measured 'total' sound and total Joule power. These were performed for driving frequencies $1\ \text{kHz} \leqslant f \leqslant 25\ \text{kHz}$.

The total sound produced by the three-branch device was measured using both voltage-based and phase-based bridging methods for different values of the branch conductances. These conductances were measured electrically by a two-terminal method. For the voltage-based method, three measurements of the total sound were recorded, one for each of $P_{1,0}$, $P_{0,1}$ and $P_{1,1}$. The conductance ratios were then determined using equation (4). The phase-based method involved varying both $|V_2|$ and φ, with $|V_1|$ held fixed. The sound was measured for $0 \leqslant |V_2| \leqslant 2|V_1|$ and $-\pi \leqslant \varphi \leqslant \pi$. The conductance ratios were then determined from equation (7).

For the two-branch device, the directivity of the far-field sound, as seen in figure 1(d), was measured for different values of G_x. Far-field sound measurements were taken by mounting the device in a rotary gimbal (Newmark Systems Inc.) and rotating the device relative to the microphone, placed multiple wavelengths away from the device.

4. Results and discussion

Figure 2(a) compares the measured total sound pressure from the three-branch device with the total Joule power. The Joule power shows excellent agreement with equation (3), including the zero points at $\varphi = \pm\pi/3$, as predicted from equation (6) when $G_1 = G_2 = G_3$. The total sound also successfully reproduces this behaviour. Figure 2(b) shows the rms difference between the total sound pressure and total Joule power as a function of the driving frequency, compared to a numerical model where the device is not assumed to behave as a point source. (The numerical model is based upon the directivity function defined in supplementary S1.) For $f < 5$ kHz there is significant error, mainly caused by $1/f$ noise in the amplifiers. The error also increases for $f > 5$ kHz. This is shown in both the model and experiment, as the point-source approximation breaks down due to diffractive effects. Experimentally, the error is further increased past this point due to scattering within the parabolic reflector setup. For $f = 5$ kHz the error was minimised, hence this was chosen as the main working frequency. The dependence of the generated sound on $|V_2|/|V_1|$, as well as φ, is shown in figure 2(c) for $f = 5$ kHz. Again, there is good agreement between experiment and model. This includes the points of zero total sound, which are indicated by vortices in the phase. The correspondence seen in all cases confirms that the total sound can be considered to be directly proportional to the total Joule power.

For the three-branch device, the measured dependence of the point of zero total sound on the branch length L is compared to equation (6) in figure 3. As L_1 decreases

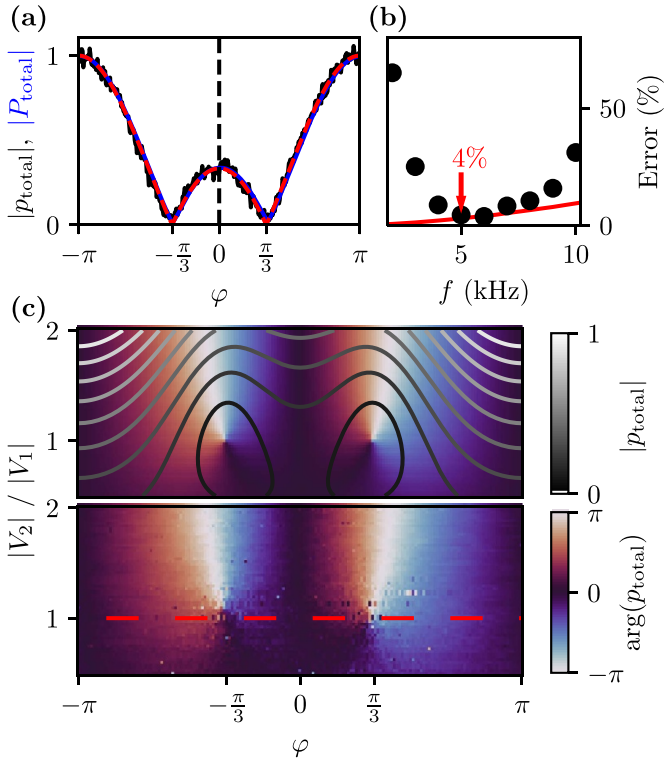

Figure 2. (a) Normalised measurements of total Joule power (blue) and total sound pressure (black) from a three-branch thermophone as a function of the phase difference φ between the voltage sources of branches 1 and 2. Here, $|V_1| = |V_2|$ and $f = 5$ kHz. Experimental data are compared with equation (3) (red). (b) The relative error between the measured $|P_{\text{total}}|$ and $|p_{\text{total}}|$ as a function of the driving frequency. The minimum is indicated by an arrow. Red line indicates simulated diffraction-based error. (c) Dependence of P_{total} and p_{total} on both $|V_2|$ and φ, with $|V_1|$ held constant. Top: modelled P_{total} from equation (3), showing both the normalised magnitude (contours) and phase (solid colour). A vortex in the phase occurs where $|P_{\text{total}}| = 0$. Bottom: experimental measurement of the phase of p_{total}. The dashed red line indicates the data shown in (a).

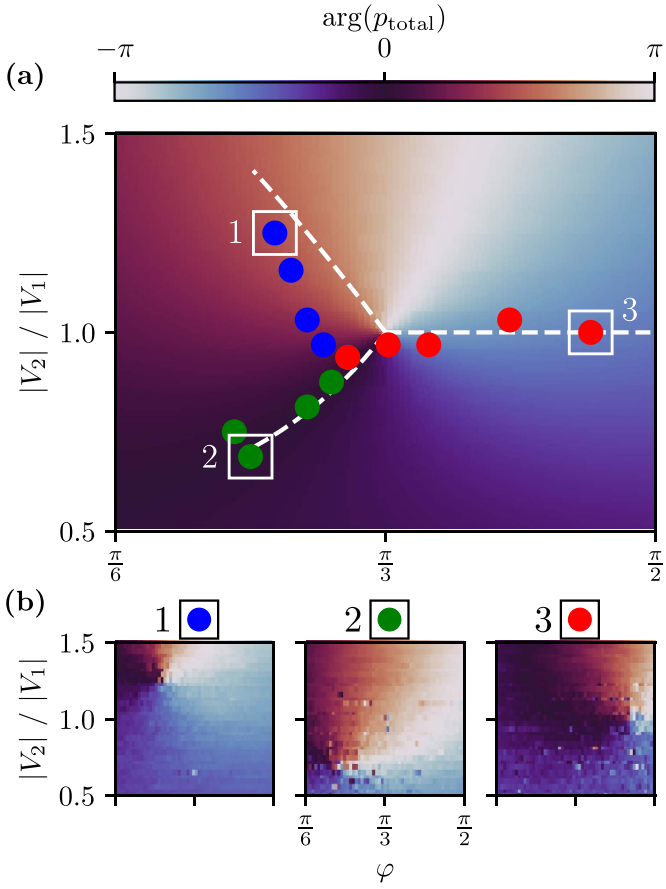

Figure 3. (a) Predicted phase of total Joule power (colourmap) as a function of relative source phase and magnitude for a three-branch device with equal branch conductances. The location of the point of zero power (phase vortex) and its dependence on individual branch conductances is shown: experimental total sound (circles) and modelled total Joule power (dashed line), where increasing conductance equates to increasing radial distance from the centre. The colours blue, red and green represent the branches 1, 2 and 3, respectively. (b) Measured total sound phase maps for the boxed points in (a).

(G_1 increases), the contribution from branch 1 to the total Joule power (hence total sound) will be reduced. In the limiting case $G_1 \to \infty$ this results in power dissipation purely from branches 2 and 3. For zero total Joule power, V_2 should then be adjusted such that $P_2 = -P_3$. In the case where $G_2 = G_3$, from equation (6) it is seen that $V_2 = \sqrt{2}V_1 e^{i\pi/4}$. This behaviour is clearly seen in the experimental data, with the zero point shifting as L_1 is decreased. Similar behaviour is observed when decreasing L_2 or L_3, where the limiting cases are $V_2 = (\sqrt{2}/2)V_1 e^{i\pi/4}$ and $V_2 = V_1 e^{i\pi/2}$, respectively. While the experimental data shows the trends predicted by the model, there is an offset in the exact locations of the zero point. This is due to the device branches having slightly different conductances per unit length, such that G_1, G_2 and G_3 are not exactly equal when $L_1 = L_2 = L_3$. The conductance ratios measured electrically and acoustically are shown in figure 4. Both voltage-based and phase-based bridging methods quantitatively agree with the direct electrical measurements. The experimental uncertainty for the voltage-based method is obtained from the standard error of the mean, as the sound measurements were averaged over a period of 60 s. For the phase-based method, the uncertainty arises from determining the location of the point of zero total sound, which can be improved by increasing the number of measurements made around the zero point. If the full behaviour of the device is measured, as in figure 3, the uncertainty can be reduced further by instead fitting with equation (3). The sensitivity of the point of zero total Joule power to the conductivity ratios inherently makes the phase-based method preferable in terms of measurement sensitivity, at the cost of increased measurement time and complexity.

In the case where the third branch is a non-sound-producing conductor of conductance G_x, the sound field formed from the other two branches is expected to be dipolar, figures 1(c) and (d). The measured directivity of the far-field sound for

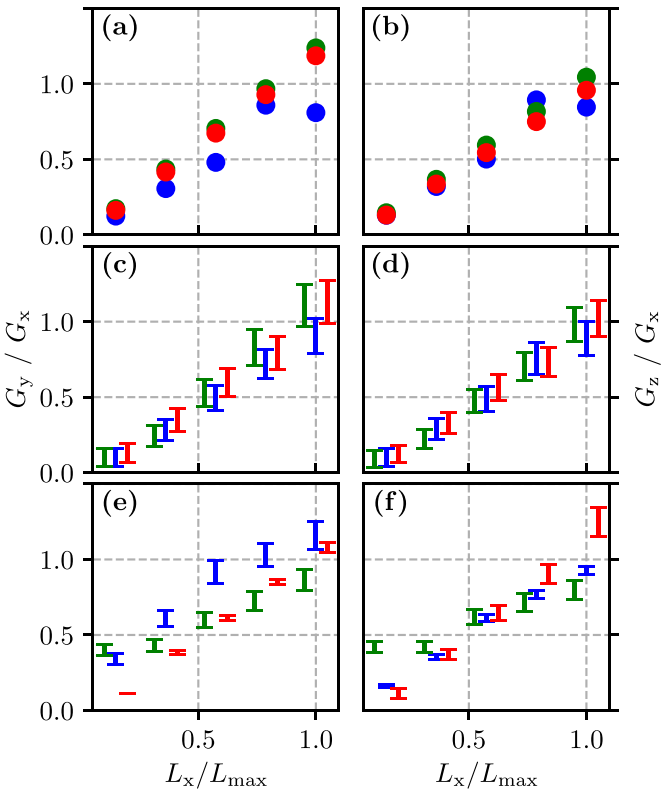

Figure 4. Measurements of three-branch device conductance ratios $G_{y,z}/G_x$ as a function of the branch lengths L_x, normalised to the maximum branch length L_{max}. Results shown for electrical measurements (a), (b), as well as the voltage- (c), (d) and phase-based (e), (f) acoustic methods. The colours blue, red and green represent $x = 1$, 2 and 3, respectively, with y and z being the other two branches in each case. The green and red data sets are horizontally shifted by 5% for visual clarity. Details for calculating the experimental uncertainties are given in supplementary sections S3 and S4, where the measurement uncertainties are calculated from time-averaged measurements and voltage sweep resolution for the voltage- and phase-based methods, respectively.

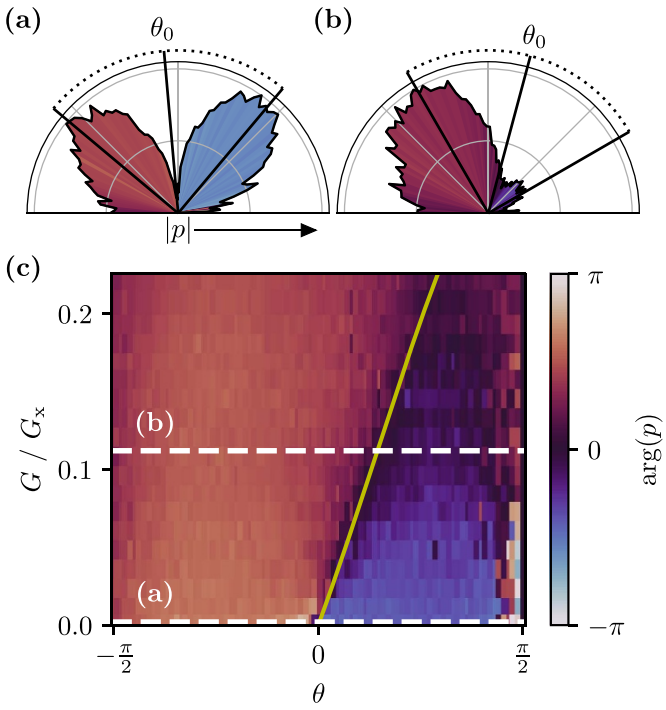

Figure 5. Far-field sound directivity as a function of conductance ratio for a two-branch device. (a) and (b) Experimental results for $G_x \gg G$ and $G_x = 0.11G$, respectively. The magnitude is indicated by the radial extent and the phase by the colour. The angle of the sound field null, θ_0, along with the positions of the lobes to either side are indicated. (c) Stacked directivity plots showing experimental sound phase as a function of conductance ratio. The expected shift of the null from equation (11) is shown by the yellow line. White dashed lines indicate the data shown in (a) and (b).

different values of G_x is shown in figure 5. When $G_x \gg G$ (figure 5(a)), a symmetric dipolar sound field is observed with a null $\theta_0 \approx 0$. A shift of this null is clearly seen as G_x is decreased (figures 5(b) and (c)). From equation (11) it can be seen that, for $kd > \pi$, the change in angle is maximised ($\theta_0 = \pi/2$) when

$$\left(\frac{G_x}{G}\right)_{min} = \frac{1-\sin\left(\frac{kd-\pi}{2}\right)}{\cos\left(\frac{kd-\pi}{2}\right)} - 1\,, \tag{12}$$

beyond which the sound field is monopolar. For $kd \leqslant \pi$ the full angular range is not used, reducing the sensitivity of the measurement and increasing the number of nulls in the sound field. Additional diffraction-based nulls will also be present when the acoustic source dimensions are larger than $2\pi/k$. It is therefore important to optimise G, k and d to achieve the best results. Since the measurement of θ_0 is angular, the precision can also be directly improved by increasing the distance between the device and the microphone.

The thermophonic bridge technique can be extended to determine the thermal properties of the thin film. Here we consider the case when the conductance is temperature dependent. For small changes around a reference temperature, T_0, the conductance can be assumed to be linear [13],

$$G(T) = \frac{G_0}{1+\alpha(T-T_0)}\,, \tag{13}$$

where α is a material constant and G_0 is the conductance at T_0. The temperature of the film is linearly dependent on the Joule power. This was verified experimentally, figures 6(a) and (b). As a result, the material constant α can be determined from measurements of the conductance at different power values. In the case where only G_3 is temperature dependent, the minimum in the total Joule power shifts in phase as a function of the temperature. This is simulated in figure 6((c), top)). Looking at the directivity of the far-field sound, a shift also occurs in the sound field null, figure 6((c), bottom). By measuring the location of this null as a function of temperature, α can be determined directly from the sound field. Moreover, as the sound also depends on the thermal conductivity and heat capacity (the proportionality constant in equation (1)) it can be used to measure these properties simultaneously with the electrical ones. As such, there is significant scope in the future to develop the thermophonic bridge into a powerful technique for precision measurements of thin-film parameters.

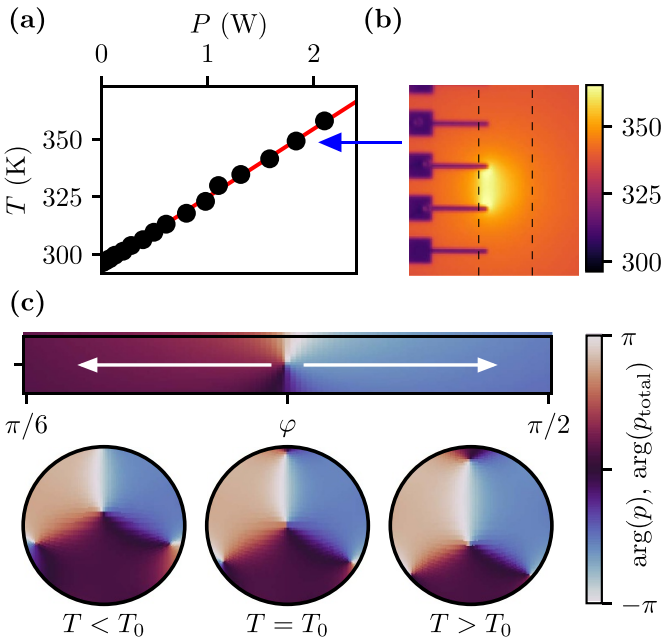

Figure 6. (a) Experimental measurement of the film temperature as a function of the Joule power. (b) Thermal image of the three-branch device at the indicated power. Dashed lines indicate film location. (c) Simulated temperature dependence of the point of zero total Joule power. Top: shift in the zero point as a function of temperature. White arrows indicate direction of shift. Bottom: orthographic projections of the far-field sound directivity at three different temperatures relative to T_0, showing a shift in the central null for $T \neq T_0$.

5. Conclusion

Branched thin-film devices configured as a thermophonic bridge can be used to determine the electrical and thermal properties of the film directly from the sound they produce. This behaviour is owed to the electrical coupling between thermophone elements, where the sound produced by each element is dependent on the properties of all other elements. By measuring the sound under different voltage driving conditions, the conductance of each branch and its temperature dependence can be determined. For the two- and three-branch devices demonstrated, the conductance measurement involves balancing the sound output from each branch. We have shown how this can be achieved using both the source magnitudes and relative phase. As with a traditional Wheatstone bridge, this only results in a relative measurement of conductance; however, we have shown how an absolute measurement can be obtained by including known conductances. The demonstration of the direct proportionality between sound and complex electrical power shows its distinctive potential for thin film characterisation. In particular, this method of balancing the circuit, in contrast to the traditional method of balancing voltages, offers a way to determine the conductance without the need for additional contacts along the branches that can perturb the measurement and limit device architecture. Furthermore, the unique, spatial aspect of this new type of bridge means that its precision can be dictated by the choice of frequency and acoustic measurement distance.

Data availability statement

The data that support the findings of this study are available upon reasonable request from the authors.

Acknowledgments

We acknowledge financial support from the Engineering and Physical Sciences Research Council (EPSRC) of the United Kingdom, via the EPSRC Centre for Doctoral Training in Metamaterials (EP/L015331/1) and QinetiQ Prosperity Partnership (EP/R004781/1).

ORCID iD

D M Tatnell https://orcid.org/0000-0003-2988-886X

References

[1] Arnold H D and Crandall I B 1917 The thermophone as a precision source of sound *Phys. Rev.* **10** 22
[2] Heath M S and Horsell D W 2017 Multi-frequency sound production and mixing in graphene *Sci. Rep.* **7** 1363
[3] Vesterinen V, Niskanen A O, Hassel J and Helistö P 2010 Fundamental efficiency of nanothermophones: modeling and experiments *Nano Lett.* **10** 5020
[4] Barnard A R, Brungart T A, McDevitt T E, Aliev A E, Jenkins D M, Kline B L and Baughman R H 2014 Advancements toward a high-power, carbon nanotube, thin-film loudspeaker *Noise Control Eng. J.* **62** 360
[5] Romanov S A, Aliev A E, Fine B V, Anisimov A S and Nasibulin A G 2019 Highly efficient thermophones based on freestanding single-walled carbon nanotube films *Nanoscale Horiz.* **4** 1158
[6] Gaal M, Bartusch J, Schadow F, Beck U, Daschewski M and Kreutzbruck M 2016 Airborne ultrasonic systems for one-sided inspection using thermoacoustic transmitters *2016 IEEE Int. Ultrasonics Symp.* (Tours: IEEE)
[7] Julius S, Gold R, Kleiman A, Leizeronok B and Cukurel B 2018 Modeling and experimental demonstration of heat flux driven noise cancellation on source boundary *J. Sound Vib.* **434** 442
[8] Tatnell D M, Heath M S, Hepplestone S P, Hibbins A P, Hornett S M, Horsley S A R and Horsell D W 2020 Coupling and confinement of current in thermoacoustic phased arrays *Sci. Adv.* **6** 27
[9] Hoffmann K 1974 *Applying the Wheatstone Bridge Circuit* (Darmstadt: HBM)
[10] Nemecek A, Oberhauser K and Zimmermann H 2006 Distance measurement sensor with pin-photodiode and bridge circuit *IEEE Sens. J.* **6** 391
[11] Tan X, Lv Y, Zhou X, Song X, Wang Y, Gu G, Guo H, Liang S, Feng Z and Cai S 2020 High performance AlGaN/GaN pressure sensor with a wheatstone bridge circuit *Microelectron. Eng.* **219** 111143
[12] Daschewski M, Boehm R, Prager J, Kreutzbruck M and Harrer A 2013 Physics of thermo-acoustic sound generation *J. Appl. Phys.* **114** 114903
[13] Ward M R 1971 *Electrical Engineering Science* (New York: McGraw-Hill)